Chiral Molecular Recognition in Small Bimolecular Systems: A Spectroscopic Investigation into the Nature of Diastereomeric Complexes

William H. Pirkle* and Thomas C. Pochapsky

Contribution from the School of Chemical Sciences, University of Illinois at Urbana—Champaign, Roger Adams Laboratory, Urbana, Illinois 61801.
Received November 17, 1986

Abstract: *N*-Aryl derivatives of α-amino esters show a high degree of chiral recognition on chiral stationary phases (CSPs) derived from *N*-(3,5-dinitrobenzoyl)-α-amino acids. Conversely, amides of *N*-(3,5-dinitrobenzoyl)-α-amino acids show similar chiral recognition on CSPs derived from *N*-(2-naphthyl)-α-amino esters. Solution ^{1}H NMR measurements of chemical shift changes as a function of concentration and temperature, UV–vis studies of charge transfer (CT) bands associated with formation of the diastereomeric complexes, and T_1 and intra- and intermolecular nuclear Overhauser effect (NOE) studies were performed on solutions of each enantiomer of *N*-(2-naphthyl)alanine methyl ester (**2b**) and (*S*)-(−)-*N*-(3,5-dinitrobenzoyl)leucine *n*-propylamide (**1b**). ^{1}H NMR and UV–vis titration studies allow the calculation of an association constant and ΔG_f, while variable-temperature ^{1}H NMR studies permit estimation of the magnitudes of ΔH_f and ΔS_f for the more stable (*S,S*) complex. Specific intermolecular NOE enhancements observed in the (*S,S*) complex corroborate the chiral recognition model proposed to account for the chromatographic separation of the enantiomers of **1b** on a CSP derived from **2** and vice versa.

For a number of years we have been investigating mechanisms of chiral molecular recognition. One aspect of this work involves designing and preparing chiral stationary phases (CSPs) for the direct chromatographic separation of enantiomers.[1] A number of the CSPs resulting from this research are now commercially available and are being increasingly used to monitor enantiomeric purity and to preparatively separate enantiomers.[2-4] The present paper describes efforts to relate the observed chromatographic separation of enantiomers on CSPs to a mechanistic understanding of chiral recognition through the use of spectroscopic techniques.

For a chiral molecule to distinguish between the enantiomers of a second species (chiral molecular recognition) a minimum of three simultaneous interactions, at least one of which is stereochemically dependent, must take place between the two species.[5] This is true of any system demonstrating chiral recognition, be it an enzyme or a CSP. Interactions may be either bonding or repulsive. Enantiomer separations on CSPs are unarguably the result of spatial factors and not due to differences in size or functionality of the analytes. Because these separations usually entail rather weak interactions which are difficult to stipulate with certainty, models accounting for observed enantiomer separations are seldom presented and may be greeted with a degree of skepticism when they are.[6] However, well-thought-out models supported by adequate evidence are of great value. They may be used to rationally approach the design of improved CSPs, select CSPs for given analytes, and relate absolute configurations of enantiomers to elution order. Good chiral recognition models also allow one to qualitatively relate given structural changes in the analyte to the magnitude of the separation factor[7] observed on chromatography on the CSP.

A major obstacle to the acceptance of chromatographically derived chiral recognition models is the indirect nature of the evidence used to support them. These models are usually inferred from a body of chromatographic data, data which represent a weighted time-average view of all interactions. Direct spectroscopic observation of CSP–analyte mixtures could provide information relevant to chiral recognition, but such experiments are complicated by the presence of the solid CSP support. By using soluble CSP analogues to interact in solution with the analyte enantiomers, the collection and interpretation of spectroscopic data is considerably simplified. While objection might be raised that the nature of chiral recognition could change in the absence of the solid support, the interactions we typically invoke to rationalize chiral recognition are those which are expected to occur in solution. In many instances, chiral recognition will be relatively independent of the presence or absence of the solid support. Even in cases where such dependence occurs, solution spectroscopic measurements can aid in understanding chiral recognition mechanisms.[7]

Recently, we reported the separation of the enantiomers of *N*-aryl-α-amino acid derivatives on a CSP, **1c**, derived from (*S*)-*N*-(3,5-dinitrobenzoyl)leucine.[8] *N*-(2-Naphthyl)alanine esters show large enantiomeric separation factors[9] (α) on this π-acceptor-substituted CSP. Since these separations are only marginally affected by changes in the length of the ester alkoxyl moiety of the analyte, it was concluded that chiral recognition between *N*-(2-naphthyl)alanine esters and CSP **1c** does not depend to any great extent on the nature or proximity of the solid support. We also note that the enantiomers of amides of *N*-(3,5-dinitrobenzyl)leucine show an even greater degree of separability on CSP **2c** derived from *N*-(2-naphthyl)alanine undecenyl ester. For example, a separation factor (α) of 15.6 is noted for butylamide **1d**.[10] The high degree of chiral recognition occurring between type **1** and type **2** compounds indicates that highly specific attractive interactions occur between enantiomers of the correct relative stereochemistry. Hence, one diastereomeric adsorbate is significantly more stable than the other. To further our understanding of the structures of these complexes, detailed spec-

(1) Pirkle, W. H.; House, D. W. *J. Org. Chem.* **1979**, *44*, 1957.
(2) Pirkle, W. H.; Finn, J. M.; Hamper, B. C.; Schreiner, J. L.; Pribish, J. R. *Asymmetric Reactions and Processes in Chemistry*; Eliel, E., Otsuka, S., Eds.; American Chemical Society: Washington, D.C., 1982; ACS Symp. Ser., No 185.
(3) Pirkle, W. H.; Hyun, M. H. *J. Org. Chem.* **1984**, *49*, 3043.
(4) Pirkle, W. H.; Pochapsky, T. C. *J. Am. Chem. Soc.* **1986**, *108*, 352.
(5) Dalgleish, C. E. *J. Chem. Soc.* **1952**, 3940.
(6) Kasai, M.; Froussios, C.; Ziffer, H. *J. Org. Chem.* **1981**, *46*, 2935.
(7) Pirkle, W. H.; Hyun, M. H.; Tsipouras, A.; Hamper, B. C.; Banks, B. *J. Pharm. Biomed. Anal.* **1984**, *2*, 173.
(8) Pirkle, W. H.; Pochapsky, T. C.; Mahler, G. S.; Field, R. E. *J. Chromatogr.* **1985**, *348*, 89.
(9) α, the chromatographic separation factor, is the ratio of the corrected chromatographic retention times of the enantiomers. The magnitude of α is related to the difference in free energy of formation of the diastereomeric adsorbates, $\Delta\Delta G_f$, by

$$\Delta\Delta G_f = -RT \ln \alpha$$

A large α reflects a high selectivity of the CSP for interaction with one enantiomer. Chiral recognition, of course, does not demand that all the interactions between the CSP and the analyte enantiomer be attractive, only that the free energies of formation ΔG_f of the two diastereomeric adsorbates be different.
(10) Pirkle, W. H.; Pochapsky, T. C.; Mahler, G. S.; Corey, D. E.; Alessi, D. M.; Reno, D. S. *J. Org. Chem.* **1986**, *51*, 4991.

0002-7863/87/1509-5975$01.50/0

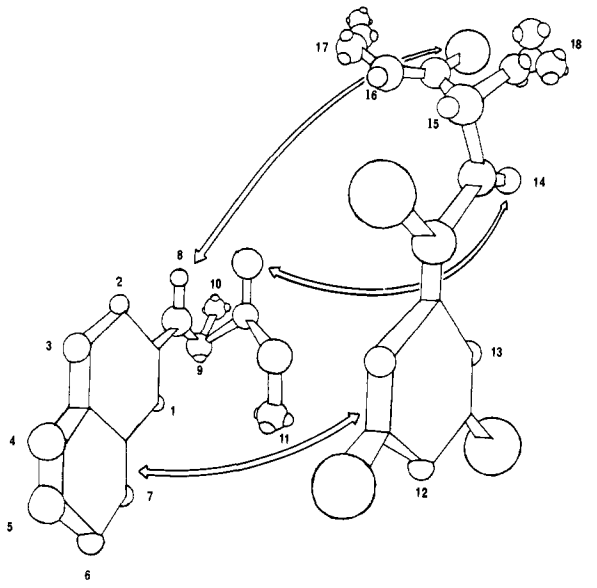

Figure 1. Chiral recognition model showing three simultaneous bonding interactions between the (*S*) enantiomers of **1b** and **2b**. The indicated interactions are as follows: a π–π interaction between the aromatic moieties, a hydrogen bond between the dinitrobenzamide proton H14 of **1b** and the carbonyl oxygen of **2b** and a second hydrogen bond between the amino *H* of **2b** and the C-terminal carbonyl oxygen of **1b**. Proton numbering refers to tabulations of ^{1}H NMR data in tables I–III.

troscopic investigations were undertaken for mixtures of type **1** and type **2** compounds.

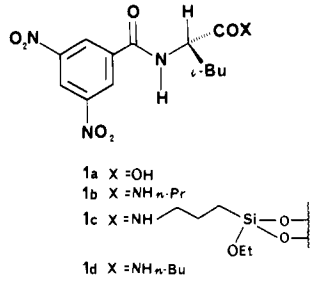

1a X = OH
1b X = NH-*n*-Pr
1c X = NH
1d X = NH-*n*-Bu

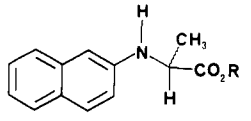

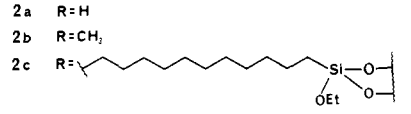

2a R = H
2b R = CH_3
2c R =

(*S*)-*N*-(3,5-Dinitrobenzoyl)leucine *n*-propylamide (**1b**) was used as the π-acceptor component because it is sufficiently soluble in nonpolar solvents to allow spectroscopic studies to be conducted at reasonable concentrations. It has a relatively simple ^{1}H NMR spectrum, and its molecular weight is low enough so that its correlation time is fairly short.[11-16]

For similar reasons, we chose methyl *N*-(2-naphthyl)alaninate (**2b**) as the π-donor component of the diastereomeric complex. Ester **2b** shows a high degree of chiral recognition on CSP **1c** (α = 9.7, 1% 2-propanol–hexane), is of low molecular weight, and has a simple ^{1}H NMR spectrum.

Figure 1 shows the chiral recognition model proposed for the more stable (*S*,*S*) diastereomeric complex of **1b** and **2b**. This is essentially the same model earlier proposed to account for the chromatographic separation of the enantiomers of type **2** analytes on CSP **1a** and for the separation of enantiomers of type **1** compounds on CSP **2c**.[8,10] The possibility for three simultaneous attractive interactions is evident. First, a π-donor–acceptor interaction is expected to occur between the highest occupied molecular orbital (HOMO) of the electron-rich 2-aminonaphthyl moiety of **2b** and the lowest unoccupied molecular orbital (LUMO) of the electron-deficient dinitrobenzoyl moiety of **1b**. The remaining two interactions are hydrogen bonds, one between the acidic dinitrobenzoyl amide proton of **1b** and the ester carbonyl of **2b**, and the other between the amino protein of **2b** and the C-terminal amide carbonyl of **1b**. One can see that by interchanging any two groups on either stereogenic center, at least one of the attractive interactions shown for the (*S*)-**1b**–(*S*)-**2b** complex will be lost.

Briefly stated, ancillary data to be offered in support of the model shown in Figure 1 are as follows: (a) the presence of a CT band in the UV–vis spectrum of the more stable (*S*,*S*)-complex arising from π-donor–acceptor interaction (this band makes it possible to establish the extent of association between **1b** and **2b** through titration experiments. Similar ^{1}H NMR titrations buttress the equilibrium constant, K_{assoc}, determined from the UV–vis absorption study and variable-temperature ^{1}H NMR studies allow determination of enthalpic and entropic contributions to the free energy of association); (b) chemical shift data that provide information on the changes occurring in local magnetic environments upon complexation of **1b** and **2b**, whereas ^{1}H T_1 experiments provide information on the effect of complexation upon spin–lattice relaxation (the latter is dependent on effective molecular size (which increases upon complexation) and the presence of nearby spin $^1/_2$ nuclei which allow T_1 relaxation to take place); and (c) a series of ^{1}H{^{1}H} nuclear Overhauser experiments which help establish both the identity of the most populated conformers of **1b** and **2b** (intramolecular NOE) and the relative orientation of the two molecules in the favored (*S*,*S*)-complex (intermolecular NOE). These intermolecular NOEs are small but specific and reproducible from sample to sample and constitute the most direct evidence to date of the validity of the chiral molecular recognition model proposed in Figure 1.[17]

Experimental Section

All reagents used were of pharmaceutical or reagent grade, and solvents used in spectroscopic studies were of spectrophotometric quality. Infrared spectra were obtained on a Nicolet Technologies 7000 FT–IR or IBM IR 32 FT–IR. Mass spectra were obtained on a Varian MAT CH-5 spectrometer with electron impact ionization. All UV–vis spectra were obtained on a Perkin-Elmer Lambda 2 digital recording spectrophotometer. All NMR experiments were performed on a Varian XL-200 FT–NMR operating at 200 MHz (proton) in the ^{2}H lock mode. All ^{13}C NMR spectra were obtained at 50 MHz by using broad-band proton decoupling. Calculations, including exact calculation and linear regression analyses of Hildebrandt-Benesi plots, were performed on an IBM PC-XT with BASIC programs written by the authors. Elemental analyses were performed by J. Nemeth and associates of the University of Illinois microanalytical service. Melting points were obtained on a Buchi melting point apparatus and are uncorrected.

Preparation of Compounds 1b and 2b. (*S*)-(–)-Methyl *N*-(2-Naphthyl)alaninate (**2b**). *N*-(2-Naphthyl)alanine (**2a**), prepared as de-

(11) Long correlation times, τ_c, would have complicated the proposed NOE experiments. The magnitude and sign of ^{1}H{^{1}H} NOE enhancements depend to a large extent on the product $\tau_c\omega_c$, where ω_c is the Larmor frequency of the resonance of concern and τ_c is a measure of the rate at which the nuclei re-orient in solution. The correlation time, τ_c, is dependent on temperature, viscosity, and molecular size. When $(\omega_c\tau_c)^2 \ll 1$, NOEs are positive and specific. That is, direct effects between two protons are seen as signal enhancements, whereas indirect effects tend to be small and negative.[12,13] When $(\omega_c\tau_c)^2$ is close to 1, NOEs are generally not observed. Very long correlation times ($(\omega_c\tau_c)^2 \gg 1$) cause spin diffusion rather than relaxation enhancement in NOE double resonance experiments, and, although transient,[14] truncated driven[15] and rotating-frame[16] NOE techniques have been developed to deal with long τ_cs, relaxation enhancement experiments are technically simpler.

(12) Noggle, J. H.; Schirmer, R. E. *The Nuclear Overhauser Effect: Chemical Applications*; Academic Press: New York, 1971.
(13) Bothner-By, A. A.; Johner, P. E. *Biophys. J.* **1978**, *24*, 779.
(14) Gordon, S. L.; Wuthrich, K. *J. Am. Chem. Soc.* **1978**, *100*, 7094.
(15) Wuthrich, K.; Wagner, G. *J. Magn. Reson.* **1979**, *33*, 675.
(16) Bothner-By, A. A.; Stepens, R. L; Lee, J.-M.; Warren, C. D.; Jeanloz, R. W. *J. Am. Chem. Soc.* **1984**, *106*, 811–813.
(17) Pirkle, W. H.; Pochapsky, T. C. *J. Am. Chem. Soc.* **1986**, *108*, 5627.

scribed previously,[18] was esterified by treatment of the free acid in absolute methanol with anhydrous HCl gas. After dissolution of the acid, the mixture was allowed to stir 1 h, after which the methanol was removed by distillation, an excess of 5% $NaHCO_3$ (aq) was added, and the crude ester, **2b**, was extracted into CH_2Cl_2. The crude ester was purified by recrystallization from hexane–CCl_4 (mp 68 °C) and separated into its enantiomers by chromatography on a preparative chiral column. A 0.5-g sample of racemic **2b** was completely resolved in one pass on an MPLC column containing 300 g of CSP **1c** covalently bonded to 40 μm Brinkmann silica. The second enantiomer eluted from CSP **1c** (0.25 g) is (*S*)-(−)-**2b**, a clear pale orange oil: ^{1}H NMR ($CDCl_3$) δ 1.53 (d, *J* = 4 Hz, 3 H), 4.28 (q, *J* = 4 Hz, 1 H), 4.34 (s (b), 1 H), 6.78 (d, *J* = 1.4 Hz, 1 H), 6.92 (dd, *J* = 1.4, 4.4 Hz, 1 H), 7.21 (m, *J* = 6.7, 7.2 Hz, 1 H), 7.36 (m, *J* = 6.7, 7.3 Hz, 1 H), 7.64 (d, *J* = 4.4 Hz, 1 H), 7.68 (d, *J* = 7.2 Hz); ^{13}C NMR ($CDCl_3$) δ 176, 136, 131, 129, 127, 123, 119, 106, 53, 20 ppm; IR (CCl_4) 3401, 2146, 3049, 2985, 2950, 2873, 2837, 1738, 1626, 1597, 1513, 1449, 1421, 1386, 1316, 1302, 1252, 1203, 1140, 1041, 963, 830, 765 cm^{-1}; UV–vis ($CHCl_3$) (ϵ_{molar}), 424 (31), 395 (61), 341 (2.17×10^3), 289 (9.36×10^3), 279 (1.12×10^4), 267 (9.99×10^3), 245 (4.37×10^4), 237 nm (5.37×10^4); mass spectrum (10 eV), *m*/*z* (rel intensity) 230 (M + 1, 5.6), 229 (M, 36.7), 171 (13.2), 170 (100). Anal. Calcd for $C_{14}H_{15}NO_2$: N, 6.11; C, 73.34; H, 5.59. Found: N, 6.09; C, 73.43; H, 6.72. $[\alpha]_D^{20}$ −159.0 (*c* 1.0, CH_2Cl_2).

(*S*)-(+)-*N*-(3,5-Dinitrobenzoyl)leucine *n*-Propylamide (1b). To 2 g (15.2 mmol) of L-leucine (Sigma) suspended in 100 mL of dry tetrahydrofuran was added 3.8 g (16.7 mmol) of 3,5-dinitrobenzoyl chloride (one portion) and 1 g (17.2 mmoles) of propylene oxide (dropwise, over 15 min). After being stirred for 2 h at room temperature under nitrogen, the solution was filtered to remove any remaining leucine, the solvent was evaporated under reduced pressure, and the crude *N*-(3,5-dinitrobenzoyl)leucine was recrystallized from acetone-CCl_4. After two crops, 4.6 g (94%) of white crystals (mp 140 °C) of **1a** were obtained. These were suspended in 50 mL of CH_2Cl_2 along with 3.88 g (15.7 mmol) of *N*-carboethoxy-2-ethoxy-1,2-dihydroquinoline (EEDQ).[19] The mixture was treated with ultrasound until solution was complete, and then an excess (5 mL) of *n*-propylamine was added. The solution grew warm and a deep purple color developed. The solution was immediately and repeatedly washed with aqueous 1 N HCl until the solution was a clear yellow. The solvent was removed under reduced pressure, and the crude **1b** was recrystallized from acetone–CCl_4. After two crops, the amide was obtained in a yield of 88% (4.6 g), mp 206 °C; IR ($CHCl_3$) δ 3415, 3280, 3100, 2958, 2936, 2875, 1655, 1645, 1545, 1463, 1345, 1074, 918 cm^{-1}; ^{1}H NMR (200 MHz, $CDCl_3$) δ 0.89–1.04 (m, 9 H), 1.55 (m, 2 H), 1.62–1.96 (m, 3 H), 3.17 (m, *J* = 5.6 Hz, 1 H), 3.36 (m, *J* = 6.2 Hz, 1 H), 4.71 (m, *J* = 8 Hz, 1 H), 6.45 (dd, *J* = 6.2, 5.6 Hz, 1 H), 8.63 (d, *J* = 8 Hz, 1 H), 8.95 (d, *J* = 2 Hz, 2 H), 9.10 (t, *J* = 1 Hz, 1 H); ^{13}C NMR ($CDCl_3$) δ 174, 164, 149, 138, 128, 122, 119, 54, 42, 26, 23, 20, 12; UV–vis ($CHCl_3$) (ϵ_{molar}) 250 (1.94×10^4), 235 nm (3.67×10^4); mass spectrum (10 eV), *m*/*z* (rel intensity) 368 (M + 2, 3.6), 367 (M + 1, 13.5), 366 (M, 2.7), 310 (92.5), 282 (75.0), 281 (100), 280 (100), 264 (21), 239 (61.8), 238 (100), 224 (62.3), 212 (43.6), 195 (100), 69 (100), 60 (94.9). Anal. Calcd for $C_{16}H_{22}N_4O_6$: C, 52.45; H, 6.05; N, 15.29. Found: C, 52.35; H, 6.21; N, 15.35. $[\alpha]_D^{20}$ +5.7 (*c* 1.0, CH_2Cl_2).

UV–vis Titrations of Solution Complexes of 1b and 2b. Samples for UV–vis spectroscopy were prepared by combining measured amounts of freshly prepared stock solutions of **1b** and **2b** in spectroscopic grade $HCCl_3$ and diluting to the appropriate concentration. Samples were prepared immediately prior to use, as solutions of **2b** darken on exposure to air and light. All measurements were obtained in a 1 cm path length quartz cell.

^{1}H NMR Studies. All $CDCl_3$ used in ^{1}H NMR studies was passed through activated basic alumina to remove traces of deuterium chloride. Samples of **1b** and **2b** for T_1 and NOE experiments were initially dried over P_2O_5 in a vacuum desiccator, dissolved in purified $CDCl_3$ under N_2, exhaustively degassed by the freeze–thaw method, and sealed under vacuum. Samples prepared in this manner showed no signs of decomposition, and the resonances of the exchangeable amine or amide protons were still visible at their original positions after several months. Although some concentration of the sample may have occurred during the freeze–thaw degassing, relative concentrations remained constant as monitored by integration of ^{1}H resonances. Care was taken that different samples were subjected to the freeze–thaw cycles under the same conditions so that any changes in concentration would occur uniformly.

All chemical shifts (δ) are reported in ppm relative to tetramethylsilane.

^{1}H NMR Chemical Shift Measurments, Titrations, and Variable-Temperature Experiments. Samples for ^{1}H NMR titrations and variable-temperature experiments were prepared similarly to those for UV–vis titrations, using $CDCl_3$ with 0.02% tetramethylsilane as the solvent. During variable-temperature experiments, care was taken to allow equilibrium of sample temperature before acquiring the FID, and concentrations of samples were calculated by taking into account the thermal coefficient of expansion of the solvent, using the function for chloroform ($V_t = V_0(1 + (1.107 \times 10^{-3})t + (4.664 \times 10^{-6})t^2 - (1.74 \times 10^{-8})t^3$).[20]

^{1}H T_1 *Measurements*. Samples for T_1 experiments were freshly prepared as described above. T_1s were measured by the inversion–recovery method and calculated with the Varian FP (find peak) and T_1 software provided with the XL-200 NMR.

^{1}H{^{1}H} Nuclear Overhauser Effect Measurements. Samples for NOE measurements were prepared as described above. Nuclear Overhauser enhancements were obtained by saturation of the desired resonance during a pre-acquisition time which was set to 10 × the longest T_1 of the resonances of interest in order to allow equilibration of state populations. This pre-irradiation period was followed by a short (0.05 s) switching time to prevent the occurrence of unwanted decoupling, followed immediately by a 90° acquisition pulse and a 2-s acquisition. Four spectra were collected with saturation at the desired resonance, followed by four reference spectra obtained identically save the irradiation occurred in an empty region of the spectrum. Typically, a total of 60–100 transients were collected at each irradiation frequency per experiment. In cases where the resonance to be saturated is a multiplet, SPT (selective population transfer) suppression techniques were used.[21] This consisted of low-power irradiation at each peak of the multiplet, each irradiation being collected as a separate free induction decay.

Difference spectra were obtained by subtraction of the reference FID from the enhanced FID, the residual FID being transformed by using a 1-Hz line broadening. In the case of multiplet irradiations (SPT suppression), all the FIDs due to multiplet irradiation are added and an appropriately weighted reference FID is subtracted. Percent enhancements were calculated by transforming the reference and enhanced FIDs and measuring integrations. All enhancements are calculated on the basis of the integration for one proton.

Results and Discussion

Differences between the solution complexes of (*S*)-**1b** and the enantiomers of **2b** are apparent to the naked eye: the diastereomeric complexes differ in color! In chloroform the (*S*)-**1b**–(*S*)-**2b** solution is dark orange, owing to the presence of a CT band (γ_{max} = 450 nm) resulting from π-donor–acceptor complex formation. This band is nearly absent in the (*S*)-**1b**–(*R*)-**2b** solution, with no maximum discernible (Figure 2). As a result, the (*R*,*S*) solution is yellow, much of this color being associated with the individual components. It is readily apparent that π-donor–acceptor complex formation is severely diminished in the (*R*,*S*) mixture.

Titration of (*S*)-**1b** with (*S*)-**2b** while monitoring either the absorbance of the CT band or chemical shift changes in the ^{1}H NMR spectrum permits one to measure the extent of complexation between (*S*)-**1b** and (*S*)-**2b**. This, in turn, allows calculation of the equilibrium constant, K_{assoc}, from two independent vantage points. The UV–vis data follow the extent of π-donor–acceptor interaction whereas the ^{1}H chemical shift data reflect changes in magnetic environment.

The Hildebrandt–Benesi method is usually used for calculating extinction coefficients and equilibrium constants of weak complexes from titration data. In expression 1

$$\frac{[C]}{A} = \frac{1}{(K_{assoc}\epsilon)}\frac{1}{[B]} + \frac{1}{\epsilon} \qquad (1)$$

A is the absorbance of the complex through 1 cm and ε is the molar extinction coefficient of the complex. One concentration, [B], is assumed to be unaffected at all concentrations of [C] by the formation of the complex, and the K_{assoc} and ε are thus obtained from the slope and *y* intercept of the graph.[22] In the present case, the assumption that the concentration of one component is unaffected by the formation of the complex is unwarranted, at least when the concentrations of **1b** and **2b** are of the same order of magnitude.

(18) Pirkle, W. H.; Pochapsky, T. C. *J. Org. Chem.* **1986**, *51*, 102.
(19) Belleau, B.; Malek, G. *J. Am. Chem. Soc.* **1968**, *90*, 1651.
(20) *Handbook of Chemistry and Physics*, 23rd ed.; Chemical Rubber Publishing Co.: Cleveland, 1943.
(21) Neuhaus, D. *J. Magn. Reson.* **1983**, *53*, 109.
(22) Benesi, H. A.; Hildebrand, J. H. *J. Am. Chem. Soc.* **1949**, *71*, 2703.

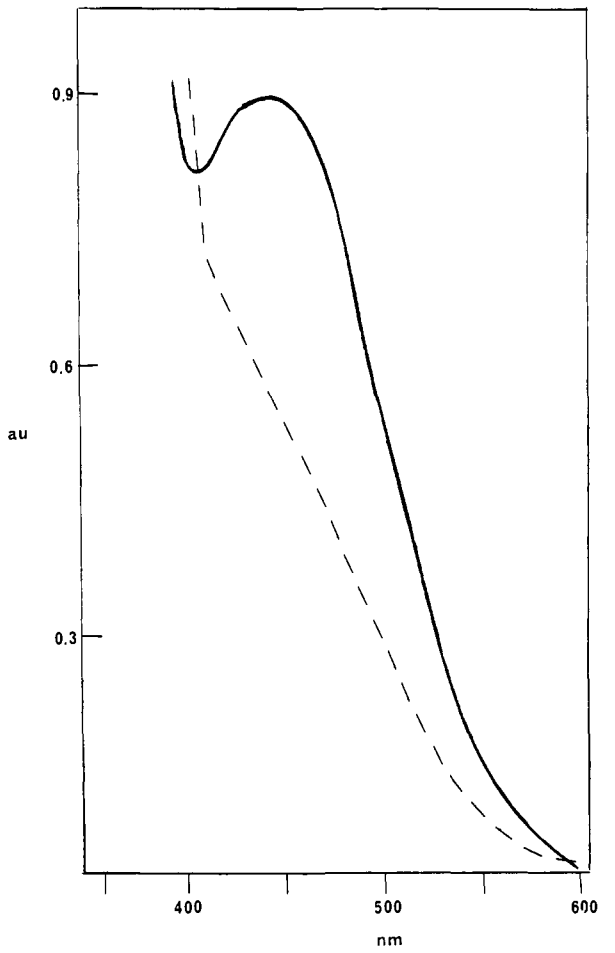

Figure 2. Ultraviolet–visible adsorption spectra of diastereomeric mixtures of **1b** and **2b**. The solid line spectrum is that of the (*S*)-**1b**–(*S*)-**2b** complex, and the dashed line is that of the (*S*)-**1b**–(*R*)-**2b** complex. Note the much greater extent to which the CT bands are developed in the (*S,S*) complex, despite the fact that the concentration of **2b** is 2× greater and the concentration of **1b** is 4× greater in the (*R,S*) than in the (*S,S*) mixture. Concentrations in the (*R,S*) mixture: [**1b**] = 0.026 M, [**2b**] = 0.012 M. Concentrations in the (*S,S*) mixture: [**1b**] = 0.012 M, [**2b**] = 0.003 M.

A further complication results from the self-association of **1b** (vide infra). Initial titration studies of the (*S,S*) complex were performed at relatively low **2b**:**1b** ratios and the initial K_{assoc} determined for the (*S,S*) complex differed from the value subsequently determined at higher ratios. ^{1}H NMR studies (vide infra) of **1b** in $CDCl_3$ solution demonstrated that the chemical shifts of many of the protons of **1b** are concentration-dependent, indicating self-association. While dimerization is expected to be the principle mode of self-association, higher aggregates may be present at high concentrations.

To more accurately determine K_{assoc} for the (*S,S*) complex, it was necessary to establish the extent to which **1b** self-associates. All of the associations described here involve fast exchange on the NMR time scale. Hence, the observed proton chemical shifts for **1b** are related to the chemical shifts of the unassociated (δ_p) and associated (δ_a) species by

$$\delta_{obsd} = \frac{C_a\delta_a + C_p\delta_p}{C_{total}} \qquad (2)$$

where C_{total} is the net concentration of all forms of the observed species, C_p is the concentration of unassociated species, and C_a is the concentration of associated species. Equilibrium constants for dimer formation of **1b** were calculated on the basis of the chemical shifts of several protons where these shifts are concentration dependent. Although the chemical shifts of amide protons H14 and H16 show the greatest concentration dependence, no simple relationship beteen these shifts and the concentration of

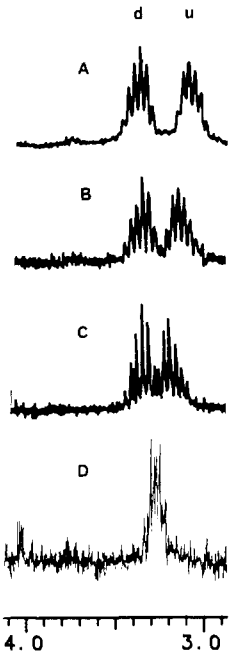

Figure 3. Chemical shift of H17 as a function of dimer formation in **1b**. Concentrations of **1b** in $CDCl_3$ at 18 °C are (A) 8.7×10^{-2} M, (B) 4.4×10^{-2} M, (C) 2.2×10^{-2} M, and (D) 4.4×10^{-4} M.

1b was found. The most reliable indicator of dimer formation was found to be the chemical shifts of H17u and H17d, the α-methylene protons of the *n*-propylamide. These protons are diastereotopic and their chemical shifts are concentration dependent (Figure 3). At very low concentrations (5×10^{-4} M), the resonances of H17u and H17d are isochronous, and A_2M_2X coupling is observed. As concentration is increased, the isochronous resonances diverge, the two signals being designated as upfield (u) and downfield (d). Increasing the concentration of **1b** leads to an increased downfield shift of H17d. Assuming the chemical shift for H17 in the 0.0005 M solution of **1b** is characteristic of the monomer, the concentration dependence of the H17d chemical shift can be related to the concentrations of dimer by eq 2. By using the expression for dimer concentration as a function of observed chemical shifts obtained from eq 2, two data sets are set equal to the equilibrium expression 3. Solving this equation for δ_A and reinsertion of δ_A into expression 3 gives an equilibrium constant $K_{dimer} = 50 \pm 10$.

$$K_{dimer} = [\text{dimer}]/[\text{monomer}]^2 \qquad (3)$$

The concentration dependence of the H17d chemical shift may result from differential shielding of the H17u and H17d protons by the dinitrobenzoyl ring of the second molecule during dimerization. The dimer is postulated to result from head-to-tail dipole-stacking interactions. As will be seen (vide infra), a nuclear Overhauser effect between the H17 protons and H13 ortho protons is consistent with that of a head-to-tail dimer.

Although dimerization of **1b** complicates the calculation of equilibrium constants for diastereomeric complex formation, it also dramatically demonstrates the relative stabilities of the (*R,S*) and (*S,S*) complexes. Because of the drastic changes in the ^{1}H spectrum of (*S*)-**2b** upon addition of (*S*)-**1b** (Table I), it is clear that the formation of the (*S,S*) complex occurs at the expense of dimer formation. Note (Table I) that the presence of (*S*)-**2b** causes the return to near-equivalence of the chemical shifts of H17u and H17d, indicating suppression of dimer formation. Conversely, the near absence of change in the spectrum of (*R*)-**2b** upon addition of (*S*)-**1b** (and the continued nonequivalence of H17 u and d) indicates that (*R,S*) complex formation does *not* compete very successfully with the dimerization of **1b**. Accordingly, calculation of an equilibrium constant for formation of the (*R,S*) complex is difficult when the concentrations of **1b** and **2b** are comparable.

Tbale I. ^{1}H Chemical Shifts (ppm) of Selected Protons in **1b** and **2b** in the Free, (*R*,*S*), and (*S*,*S*) Mixtures[a]

proton	free	*R*,*S*	*S*,*S*
H1	6.78	6.76	6.33
H2	6.92	6.89	6.65
H3	7.64	7.58	7.2–7.3
H4	7.68	7.63	7.37
H5	7.21	7.18	7.03
H6	7.36	7.34	7.2–7.3
H7	7.61	7.56	7.2–7.3
H8	4.34	4.70	5.68
H9	4.28	4.28	4.23
H10	1.53	1.53	1.63
H11	3.74	3.74	3.95
H12	9.10	8.98	8.52
H13	8.95	8.92	8.73
H14	8.63	8.92	8.75
H15	4.71	4.72	4.62
H16	6.45	6.76	6.73
H17u	3.17	3.13	3.30
H17d	3.36	3.34	3.34

[a] All shifts are measured relative to tetramethylsilane in $CDCl_3$ at 18 °C. Concentration is 0.043 M for all components. Shifts are reported for the center of multiplets. Coupling constants and integration are reported in the Experimental Section.

In order to determine the true K_{assoc} for the (*S*,*S*) comples, it was necessary to perform all titrations at high **2b**:**1b** ratios. Complex formation was monitored at two wavelengths, 550 and 525 nm. Although the (*S*,*S*) complex exhibits a distinct maximum at 450 nm, this maximum lies close to the longer wavelength absorption maxima of uncomplexed **2b**. Hence, complex formation was monitored at longer wavelengths. A plot of absorbance data obtained at 550 nm for the (*S*,*S*) complex affords a linear Hildebrandt–Benesi plot with a fairly good correlation coefficient (R = 0.98). From the plots, an extinction coefficient (ϵ_{550} = 104.5) was calculated for the complex at 20 °C. This in turn yields an equilibrium constant, K_{assoc} = 88.17, where

$$K_{assoc} = \frac{[(S)\text{-}\mathbf{2b}\text{–}(S)\text{-}\mathbf{1b}]}{[(S)\text{-}\mathbf{1b}][(S)\text{-}\mathbf{2b}]} \quad (4)$$

Equilibrium constants for the (*S*,*S*) complex were also obtained from ^{1}H NMR chemical shifts as a function of concentration and temperature. Again, the apparent chemical shifts were related to the shifts of the pure component (δ_p) and the shifts of the complex (δ_c) by eq 2. Figure 4 is a plot of chemical shift of the para proton, H12, of the dinitrobenzoyl ring of **1b** as a function of **2b** concentration and temperature. We chose this proton to monitor as its chemical shift shows little concentration dependence in the absence of **2b** but a large dependence on the concentration of **2b** owing to π-donor–acceptor interaction. The chemical shift of H12 must therefore reflect the ratio of complexed to uncomplexes **1b**, whether the uncomplexed **1b** is present as monomer, dimer, or some higher order aggregate.

The equilibrium constants (a), (b), and (e) listed in Figure 4 for the (*S*,*S*) complex were calculated by equating two data sets obtained at high **2b**:**1b** ratio and solving the resultant quadratic equation for δ_c of H12. Constants (c) and (d) were estimated by using the calculated δ_c from (b). The average values ΔH_{assoc} = –4.75 kcal/mol and ΔS_{assoc} = –7 cal/(mol K) were calculated from constants (a), (b), and (e). In each case, the fit of experimental data to the calculated curves is best at high **2b**:**1b** ratios and worsens as more of the available **1b** is present as dimer. Attempts to deconvolute the relative contributions of complex and dimer to the observed values were only partially successful. At low relative concentrations of **2b**, dimer formation, as estimated by using the equilibrium constant calculated above, does not completely account for the discrepancy between the observed chemical shifts and those calculated from $K_{assoc(S,S)}$. For this reason, we suspect that **1b** is capable of higher order self-associations. Nevertheless, at higher **2b**:**1b** ratios, the concentration of the (*S*,*S*) complex follows that calculated from the equilibrium constant quite well and data from both the UV–vis (K = 88 at 20 °C) and ^{1}H NMR (K = 103 at 20 °C) experiments are in fairly close agreement as to the value of $K_{assoc(S,S)}$.

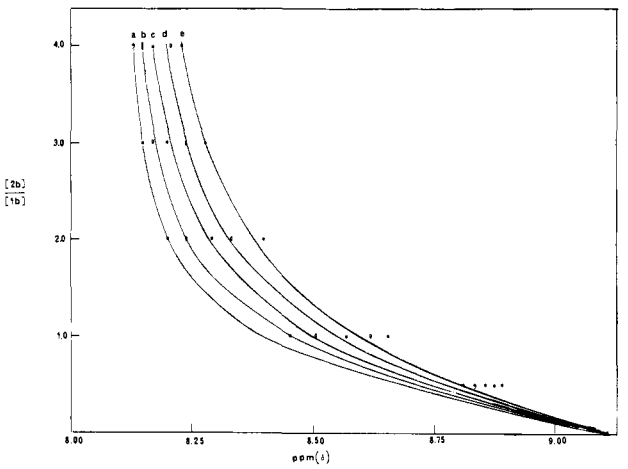

Figure 4. Chemical shift of the para proton H12 on the dinitrobenzoyl ring of (*S*)-**1b** as function of temperature and the ratio of the concentrations of (*S*)-**2b** and (*S*)-**1b**. Solid lines are plots of calculated best fit K_{assoc} for the (*S*,*S*) complex, with the experimental data points shown. Concentrations have been adjusted for the thermal expansion of chloroform. Concentration of (*S*)-**1b** was always 0.020 M (293 K) in $CDCl_3$, and the concentration of (*S*)-**2b** varied. (a) 216 K, K_{assoc} = 341.4, calcd δ_{comp} = 8.80, δ_{free} = 9.11. (b) 226 K, K_{assoc} = 241.7, calcd δ_{comp} = 8.09, δ_{free} = 9.11. (c) 276 K, K_{assoc} = 175.5, calcd δ_{comp} = 8.09, δ_{free} = 9.10. (d) 286 K, K_{assoc} = 130.3, calcd δ_{comp} = 8.09, δ_{free} = 9.10. (e) 296 K, K_{assoc} = 98.8, δ_{comp} = 8.09, δ_{free} = 9.10.

The values for ΔH_{assoc} and ΔS_{assoc} mentioned above are admittedly derived from a limited amount of data and are largely of qualitative significance. However, the value for ΔH_{assoc} is reasonable for the interactions invoked in the chiral recognition model: two hydrogen bonds (each of ca. –2 kcal/mol)[23] and a π-donor–acceptor complex (ca. –1 kcal/mol).[24] Although the ΔH for formation of strong hydrogen bonds can be as great as –6 kcal/mol, some compromise in individual bond strength might be expected in order to minimize the energy of the complex (i.e., no single interaction need be maximized).

^{1}H Chemical Shift Studies. An examination of Table I indicates large changes in local magnetic environments upon formation of the (*S*,*S*) complex. Noticeable upfield shifts occur for the aromatic protons of both species, since each aromatic system is shielded by the other in the complex. The average upfield shift in the 0.043 M mixture is 0.3 ppm, the largest effect (0.58 ppm) being seen at para proton H12 of **1b**. The 0.043 M (*R*,*S*) mixture shows little change in the chemical shifts the aromatic protons relative to the separate components. The small shifts observed for H2 ($\Delta\delta$ = –0.04), H3 ($\Delta\delta \simeq$ –0.06), and H4 (–0.05 ppm) (Figure 2) may be occasioned by factors other than π–π interaction. As do the UV–vis data, ^{1}H NMR data clearly indicate that negligible π–π interaction occurs in the (*R*,*S*) mixture.

Amino proton H8 of **2b** and amide protons H14 and H16 of **1b** are potential sites for hydrogen bonding. In the (*S*,*S*) mixture, the H8 signal is shifted 1.3 ppm downfield. A much smaller shift ($\Delta\delta_{H8}$ = +0.17) occurs in the (*R*,*S*) mixture. This indicates that H8 participates more extensively in hydrogen bonding in the (*S*,*S*) mixture than in the (*R*,*S*) mixture. For amide protons H14 and H16, as in the case of dimer formation, the implications of the data are not so clear. For dinitrobenzamide proton H14, a greater downfield shift is seen in the (*R*,*S*) mixture than in the (*S*,*S*) mixture ($\Delta\delta_{H14}(S,S)$ = +0.12, $\Delta\delta_{H14}(R,S)$ = +0.28), while the C-terminal carboxamide proton H16 shows nearly equal shifts ($\Delta\delta_{H16}$ = +0.31) in the (*R*,*S*) and ($\Delta\delta_{H16}$ = +0.28) in the (*S*,*S*) mixture. It is possible that amide proton H16 actually participates

(23) March, J. *Advanced Organic Chemistry*, 3rd ed.; J. Wiley and Sons: New York, 1985.
(24) Merrifield, R. E.; Phillips, W. D. *J. Am. Chem. Soc.* **1958**, *80*, 2778.
(25) Balaram, P.; Bothner-By, A. A.; Breslow, E. *Biochemistry* **1973**, *12*, 4695.

Table II. Proton T_1 Relaxation Times (s) for Selected Protons in **1b** and **2b** in the Free, (*R*,*S*), and (*S*,*S*) Mixtures[a]

proton	free	*R*,*S*	*S*,*S*
H1	3.0		1.1
H2	3.4	2.0	1.0
H5	6.2	3.2	1.8
H6	5.3		
H7	4.6	2.7	1.8
H9	2.8	1.5	0.9
H11	3.5	2.4	1.4
H12	12.2		11.0
H13	2.0	1.5	1.3
H14	0.4		0.4
H15	0.4	0.4	0.6
H16	0.6		0.4
H17u	0.7	0.6	0.8
H17d	0.7	0.6	0.7

[a] Concentrations of all components are 0.043 M at 18 °C in $CDCl_3$.

in hydrogen bonding to a greater extent in the (*R*,*S*) mixture than in the (*S*,*S*) mixture for, in the (*S*,*S*) complex, no single interaction need be maximized. That is, individual interactions "compromise" to minimize the energy of the complex. In the (*R*,*S*) complex, the need to "compromise" is reduced.

Amide proton H16 is not implicated in the chiral recognition scheme of interactions. The downfield shifts noted for H16 may result simply from the increase in concentration of basic hydrogen bonding sites upon addition of **2b**. The similarity in the downfield shifts of H16 in the two diastereomeric mixtures can be taken to imply that H16 hydrogen bonding may occur but that it is nonspecific and unimportant to chiral recognition.

Other chemical shift differences noted between the (*R*,*S*) and (*S*,*S*) mixtures include those for methoxyl protons H11 of **2b**. No shift occurs in the (*R*,*S*) mixture whereas a shift of −0.2 ppm is noted for the (*S*,*S*) mixture. This latter shift may be ascribed to withdrawal of electron density from the carbomethoxy group of **2b** by hydrogen bonding between its carbonyl oxygen and H14. Alternatively, the H11 protons might lie in the deshielding region of the dinitrobenzoyl ring of **1b** in the (*S*,*S*) complex.

Finally, the reader will recall that in the (*S*,*S*) mixture, the two resonances for H17u and H17d are essentially isochronous, indicating suppression of dimer formation for **1b**. In contrast, these signals remain anisochronous in the (*R*,*S*) mixture, with almost no chemical shift changes occurring.

^{1}H T_1 Relaxation Studies. Table II presents proton relaxation times for **1b**, **2b**, and the (*R*,*S*) and (*S*,*S*) mixtures. Although these measurements were made primarily to determine delay times for NOE experiments, it is clear from the table that formation of the (*S*,*S*) complex considerably reduces T_1 for many of the protons of **1b** and **2b**. This most likely results from the increased molecular correlation times, τ_c, for the (*S*,*S*) complex because of the increase in its effective molecular size. The shorter T_1s are not merely manifestations of some concentration effect since an otherwise identical (*R*,*S*) mixture does not show comparable reductions. Interestingly, formation of the (*S*,*S*) complex actually increases T_1 for H15, H16, and H17u and H17d. This may stem from the decreased interaction between these "backbone" protons and the side-chain protons of **1b**, resulting in less efficient dipolar relaxation.

^{1}H{^{1}H} Nuclear Overhauser Effect Studies. Bothner-By and co-workers have described the equilibrium magnetization, m_t, of a A + B ↔ AB system at fast exchange by

$$m_t = \frac{fT_c m_f + cT_f m_c}{fT_c + cT_f} \quad (5)$$

where signal strength is proportional to the magnetization m_t, and f and c are the mole fractions of free and complexes forms of the observed species, respectively. T_f^{-1} and T_c^{-1} are the rates of approach to equilibrium of magnetizations in the free and bound forms, respectively, and m_f and m_c are the equilibrium magnetizations of the observed resonance in the free and bound forms.[25] The amount of intermolecular NOE seen is dependent on the mole fraction of complexes species and the spin–lattice relaxation rates in the free and bound forms (assuming that, in the absence of a strong irradiating field, the spin temperature of the free and bound forms are the same). In the present case, the fraction of free and bound **1b** and **2b** may be calcuated by using 2 and the complexation-dependent chemical shift of H12. At the concentrations used, the signal of H12 is at δ 8.52 in the (*S*,*S*) mixture. Using the free chemical shift of H12 (δ_f = 9.10) and the calculated shift for H12 in the complex (δ_c = 8.09), one determines that 58% of **1b** is complexed in the 0.043 M solution. On the basis of the measured T_1s for H12 free and in the (*S*,*S*) mixture, T_1s for the complex may be calculated. From these T_1 values and the concentration of complex in the (*S*,*S*) mixture calculated from K_{assoc}, eq 5 allows one to estimate the actual magnitudes of the intermolecular NOEs to be about 60% of the NOEs expected if **1b** and **2b** were completely complexed. Although this estimate assumes a number of ideal circumstances (complete saturation of the target resonance, only dipole–dipole contributions to T_1, and that complex formation is "on–off", reducing random effects), one concludes that substantial intermolecular NOEs can be expected in the (*S*,*S*) complex.

We first will discuss the intramolecular NOEs observed since they provide valuable clues as to the conformations of **1b** and **2b** in the diastereomeric complexes. For example, saturation of H9 on the chiral center of **2b** gives rise to nearly equal effects at H1 and H2 on the naphthyl ring (7.3% and 4.2%, respectively) in the (*R*,*S*) mixture, indicating that there is little orientational preference of the naphthyl ring syn or anti to H9 in the (*R*,*S*) complex. The same experiment on the (*S*,*S*) mixture indicates a strong preference of the naphthyl ring system for the syn orientation with respect to H9 shown in Figure 1 (NOEs 10.2% for H1 vs. 1.9% for H2). This preference is most likely due to improved HOMO–LUMO overlap in the π-donor–acceptor complex resulting from this orientation of the naphthyl ring. Since this orientation also places amino proton H8 closest to H2 on the naphthyl ring, a large NOE should be, and is, seen at H2 upon saturation of H8 (NOEs 5.4% to H2 and 2.3% to H1 in the (*S*,*S*) mixture). Saturation of H8 also gives rise to a fairly large negative NOE (−9.5%) at proton H9. This is the only major negative NOE seen in these experiments and is probably due to indirect effects in the multiple spin system which includes H1, H2, and H8 and H9.

Turning attention to intramolecular effects in **1b**, a number of interesting interactions are seen. The trans arrangement of the amide protons of **1b** shown in Figure 2 is substantiated by large NOEs between C-terminal amide proton H16 and the proton on the chiral center H15, with lesser effects between H14 and H15). As indicated above, NOEs between the dinitrobenzoyl ring protons and the isobutyl methyl protons, H18, in the free form indicate that in the absence of (*S*,*S*)-complex formation, the side-chain protons of **1b** provide an important relaxation path for the "backbone" protons of **1b**. Less obvious are the NOEs seen between the H17 protons on the α-carbon of the C-terminal *n*-propylamide side chain of **1b** and the dinitrobenzoyl ring protons, H12 and H13. In the same category are the differential NOEs seen between H17 u and d upon saturation of the amide proton H16 in the free and (*R*,*S*) mixture. These effects are always greater for H17u than for H17d. To explain these NOEs, we once more invoke the head-to-tail **1b** dimer. Dimerization brings the C-terminal *n*-propylamide chain into close proximity to the dinitrobenzoyl ring, inducing the chemical shift differences noted earlier. It also gives rise to NOEs between H17 and the dinitrobenzoyl ring protons H12 and H13. Since H17u is, on a time-average basis, gauche with respect to amide proton H16 while H17d is anti to H16, saturation of H16 leads to larger NOEs at H17u than at H17d.

From inspection of Table III, one immediately notes that intermolecular NOEs are seen only in the (*S*,*S*) complex, with one exception: irradiation of methoxy protons H11 of **2b** gives rise to an NOE at the o-ring proton, H13, of **1b** in the (*R*,*S*) complex. As stated above, the chemical shift of the dinitrobenzamide proton H14 changes substantially upon formation of the (*R*,*S*) complex, and formation of a hydrogen bond between H14 and the carbonyl

Table III. Intra- and Intermolecular NOE in the Free, (*R*,*S*), and (*S*,*S*) Mixtures of **1b** and **2b** at 18–20 °C [All Enhancements (Unless Otherwise Noted) Are Positive]

irradiated		intramolecular NOE	intermolecular NOE
H1	(free)	H7 (4.6), H9 (3.0)	
	(*R*,*S*)	H7 (7.7), H9 (4.0)	
	(*S*,*S*)	H7 (13.3), H9 (10.1)	H13 (1.8)
H2	(free)	H3 (11.8), H9 (9.1)	
	(*R*,*S*)	H3 (6.2), H9 (1.3)	
	(*S*,*S*)[a]	H8 (1.4), H9 (2.2) H3 (7.6)	H13 (0.8)
H5	(*S*,*S*)	H4 (9.0)	H12 (1.5)
H8	(*R*,*S*)[b]	H1 (3.9), H2 (5.4)	
	(*S*,*S*)	H1 (2.3), H2 (5.4), H9 (−9.5)	H17d (−1.1)
H9	(*R*,*S*)	H1 (7.3), H2 (4.8), H10 (1.6)	
	(*S*,*S*)	H1 (10.2), H2 (1.9), H10 (1.7)	
H11	(*R*,*S*)		H13, H14 (1.6)
	(*S*,*S*)	H1 (7.9), H2 (4.6)	H13 (1.8)
H12	(*R*,*S*)[e]	H15 (4.4), H16 (0.9)	
	(*S*,*S*)		H5 (3.1), H6[d] (1.9)
H13	(*R*,*S*)[e]	H15 (4.4), H16 (0.9)	
	(*S*,*S*)[f]	H15 (5.6)	H1 (4.8), H2 (1.8), H7[g] (3.9), H11 (1.0)
H14	(*R*,*S*)[e]	H15 (4.4), H16 (0.9)	
	(*S*,*S*)[f]	H15 (5.6)	H1 (4.8), H2 (1.8), H7[g] (3.9), H11 (1.0)
H15	(free)	H14 (1.8), H16 (7.3)	
	(*R*,*S*)[b]	H14 (1.2), H16 (3.9)	
	(*S*,*S*)	H16 (4.0)	
H16	(free)	H15 (14.0), H17u (2.3), H17d (1.8)	
	(*R*,*S*)	H15 (10.0), H17u (3.0), H17d (2.5) isobutylmethylene of **1** (2.6)	
	(*S*,*S*)[a]	H15 (9.4)	
H17	(*R*,*S*)	(u) H13 (1.9)	
	(*S*,*S*)	H12 (4.8), H13 (2.1), H16 (2.7)	H1 (0.5), H2 (2.1), H3, H4[h] (2.1)

[a] H2 and H16 are isochronous in the (*S*,*S*) mixture. [b] H8 and H15 are isochronous in the (*R*,*S*) mixture. [c] H13 and H14 are isochronous in the (*S*,*S*) mixture, so NOE assignment is tentative. [d] H6, H7, H4, and H3 are grouped together in the (*S*,*S*) mixture, and identification of the H6 resonance was made by NOE from H5. [e] H12, H13, and H14 are isochronous in the (*R*,*S*) mixture. [f] H13 and H14 are isochronous in the (*S*,*S*) mixture. [g] Identification of the H11 resonance was by NOE from H1 (see note *d*). [h] A number of NOEs for the naphthyl ring protons of **2b** in the (*S*,*S*) mixture stem from irradiation of H17u and H17d. These occur in the crowded 7.2–7.3-ppm region, so assignments are tentative.

of **2b** would bring H13 and the methoxy protons H11 into proximity. This interaction is probably the strongest in the (*S*,*S*)-complex as H14 is relatively acidic owing to the inductive effect of the dinitrobenzoyl system. This bond is apparently the interaction least likely to be sacrificed in the (*R*,*S*) complex, and the maintenance of this hydrogen bond is evidenced by the NOE observed.

It is not surprising that most of the intermolecular NOEs in the (*S*,*S*) complex are observed for the aryl ring protons of **1b** and **2b**, these being the least efficiently relaxed protons in the system (see Table II). Although some difficulty was encountered in assigning NOE in the crowded δ 7.2–7.3 region of the naphthyl system of **2b**, enough unambiguous NOEs were obtained from free-standing resonances to allow establishment of the relative orientations of the naphthylamino and dinitrobenzoyl ring systems in the (*S*,*S*) complex. The accurate determination of the relative orientations of the two aromatic systems involved in the (two-point) π-donor–acceptor interaction in turn gives a great deal of information regarding the relative positions of the chiral centers in the complex. From Table III, it will be noted that saturation of the dinitrobenzoyl *o*-protons H13 and amide proton H14 gives rise

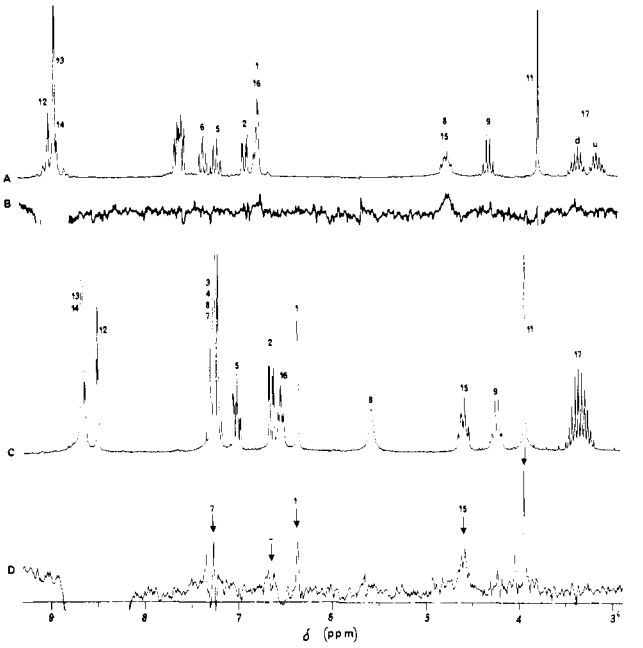

Figure 5. Intra- and intermolecular NOE in diastereomeric complexes of **1b** and **2b**. All spectra were obtained at 18 °C, at nominal concentrations of 0.043 M for all components in $CDCl_3$. Spectra are scaled in ppm relative to tetramethylsilane. (A) 0.043 M (*R*)-**2b** + 0.0.043 M (*S*)-**1b**. (B) NOE difference spectrum obtained upon saturation of the dinitrobenzoyl ring and amide protons of **1b**. Note the absence of intermolecular effects. (C) 0.043 M (*S*)-**2b** + 0.043 M (*S*)-**1b**. (D) NOE difference spectrum obtained upon saturation of the o-ring protons H13 and amide proton H14 of **1b** (ca. 20% signal loss on p-proton H12 was seen due to decoupler band width). Note intermolecular effects at H7?, H2, H1, and H11 of **2b** as well as in intramolecular effect at H15. Intensities of effects are listed in Table III.

to NOEs at H1 (4.8%), H2 (1.8%), and at carbomethoxy protons H11 (1.0%). Another fairly large NOE in the δ 7.2–7.3 region is tentatively assigned to H7, based on the intramolecular NOE observed upon saturation of H1. This experiment, shown in Figure 5, substantiates the relative relationships shown in Figure 2: One of the H13 protons and the amide proton, H14, lie close to H1 in the (*S*,*S*) complex, and the other H13 proton will lie near H2. Hydrogen bonding between H14 and the carbonyl of **2b** will also bring the carbomethoxy protons, H11, close to the dinitrobenzoyl ring system, as the observed NOE indicates. The reverse effects are observed as well: Saturation of the resonance assigned to H1 gives an NOE at H13 (1.8%). Saturation of the carbomethoxy protons, H11, of **2b** gives an NOE at H13 (1.8%). A small but specific NOE was observed at H12 upon saturation of the H5 multiplet of **2b** with no effect at H13 or H14. The reverse effect is also seen: Saturation of the H12 resonance gives no effect at H1 or H2, but enhancements are seen at H5 (3.1%) and at one resonance inthe crowded δ 7.2–7.3 region, tentatively assigned to H6. Finally, saturation of the *n*-propyl α-methylene protons H17 of **1b** gives rise to NOEs at naphthyl ring protons H1 (0.5%) and H2 (2.1%) and tentatively assigned effects at H3 and H4 (total enhancement 2.1%). Referring again to Figure 1, H2 is the proton on the naphthyl ring closest to the hydrogen bond between the amino proton H8 and the C-terminal carbonyl of **1b**, bringing H2 close to the H17 protons.

Conclusions

The enantiomeric separation of compounds of type **2** on CSP **1c** and the inverse separation of compounds of type **1** on CSP **2c** have been explained with use of a chiral molecular recognition model derived from chromatographic data. Direct spectroscopic observation of a soluble version of this system substantiates the basic model and adds further detail as to conformational preference during complexation. Concerned that the nature of the chiral recognition might differ in the NMR and chromatogrphic systems owing to the use of different solvents (all chromatographic work

referred to here was conducted with an 2-propanol–hexane mobile phase), we utilize chloroform as a mobile phase for the separation of the enantiomers of **2b** on CSP **1c**. Despite rapid elution of both enantiomers, the same sense of chiral recognition and a large (though reduced) separation factor ($\alpha > 4$) were observed.

In a publication dealing with the separation of enantiomers on CSP **2b**, we show that the presently supported chiral molecular recognition model can be extended to encompass the separation and sense of recognition observed for the 3,5-dinitrobenzoyl derivatives of a large number of chiral amines and alcohols.[10]

We conclude that spectroscopic experiments with soluble analogues of CSPs are a useful adjunct to chromatographic data for establishing the mechanisms by which enantioselectivity occurs. NOE experiments are especially powerful in ascertaining the structure of transient complexes and are capable of providing information regarding conformational preferences in the complex. However, *intermolecular* NOE experiments will not be successful in all cases, since a very high degree of association seems essential. By using chromatographic data to choose analytes for study, it is clear that many other systems suitable for successful intermolecular NOE studies can be found.

Acknowledgment. This work has been supported by a grant from the National Science Foundation and the Eli Lilly Corp.

^{7}Li, ^{29}Si, ^{119}Sn, and ^{207}Pb NMR Studies of Phenyl-Substituted Group 4 Anions

Ulf Edlund,*† Tore Lejon,† Pekka Pyykkö,‡ T. K. Venkatachalam,⊥ and Erwin Buncel*⊥

Contribution from the NMR Research Group, Department of Organic Chemistry, Umeå University, S-90187 Umeå, Sweden, Department of Chemistry, University of Helsinki, SF-00100 Helsinki, Finland, and Department of Chemistry, Queen's University, Kingston, Canada K7L 3N6. *Received January 23, 1987*

Abstract: The ^{7}Li, ^{29}Si, ^{119}Sn, and ^{207}Pb chemical shifts of phenyl-substituted group 4 anions are reported as a function of solvent and counterion. Generally, upfield shifts are noted on increasing the anion–alkali metal interaction. With additional support from ^{7}Li NMR results, it is argued that the lithium–group 4 atom interaction, including carbon, increases as the size of the group 4 element decreases. However, if the cation solvation is increased, the following order for the anion–cation interaction is obtained: C ~ Pb < Sn < Ge < Si. The increased delocalization upon solvation, which is important for the carbanion only, will thus decrease the electrostatic interaction considerably. A significant interaction between silicon and lithium is also consistent with the existence of scalar Si–Li coupling. ^{207}Pb chemical shifts of plumbyl anions are reported for the first time, and the resonances appear in an extreme low-field range. Large Pb–C scalar couplings are also noted for plumbyl anions. The chemical shifts are discussed by using a simple, relativistic extended Hückel model for PbH_3^- and the relativistic analogue of Ramsey's theory. The Pb 6s atomic orbitals (AO's) are found to be potentially important. The validity of a classical ion pair description of these group 4 anions is illustrated by a multivariate data analysis approach.

The role of covalency in group 4 atom–alkali metal interactions has mostly been studied in carbanion systems,[1] but a few NMR reports exist where both Si–Li and Ge–Li compounds have been examined.[2,3] Considering the ^{29}Si chemical shift data reported earlier, no systematic substituent effects were revealed that could shed light on the Si–Li bonding.[3a] In another study, however, strong resemblances between the C–Li and the Si–Li (Ge–Li) bond have been suggested, based on ^{7}Li chemical shift differences.[3d] It was also found that inversion about the Si (Ge) atom was slow on the ^{1}H NMR time scale, by using diastereotopic groups attached to the silicon atom.[3d] From ^{1}H and ^{7}Li NMR chemical shifts, it was suggested by Cox et al. that the degree of association between the group 4 atom and the lithium increases in the order Pb < Sn < Ge ~ Si.[2a] These authors also suggestd a considerable degree of covalent character in the lithium–group 4 atom bond for the silyl and germyl compounds. An independent study by other workers gave additional support for this trend of interaction between lithium and these group 4 elements.[2b]

Using mainly ^{13}C and $^{6(7)}Li$ NMR spectroscopy, we have investigated charge delocalization/polarization in phenyl-substituted group 4 anions,[4a-d] in continuation of our spectroscopic studies of benzylic-type carbanions.[4e-j] Contrary to the situation for the carbanion analogues, it was concluded that the excess charge resides almost exclusively on the group 4 element.[4a,b] The observed ^{13}C chemical shift changes could be satisfactorily explained by π-polarization as the mode of transmission of negative charge. Changing the counterion, or solvent, could modulate this effect to some extent. It was shown that in ethereal solution the silicon–cation interaction was equal or greater than that for the C–Li bond in Ph_3CLi in diethyl ether (DEE).[4a] Both ^{13}C chemical shift data and ^{7}Li chemical shifts supported this conclusion. A major contribution from tight ion pairing was also indicated for the

† Umeå University.
‡ University of Helsinki.
⊥ Queen's University.

(1) (a) Seebach, D.; Hässig, R.; Gabriel, J. *Helv. Chim. Acta* **1983**, *66*, 308. (b) Seebach, D.; Gabriel, J.; Hässig, R. *Ibid.* **1984**, *67*, 1083. (c) Hässig, R.; Seebach, D. *Ibid.* **1983**, *66*, 2269. (d) Fraenkel, G.; Henrichs, M.; Hewitt, J. M.; Su, B. M.; Geckle, M. J. *J. Am. Chem. Soc.* **1980**, *102*, 3345. (e) Beckenbaugh, W. E.; Geckle, J. M.; Fraenkel, G. *Chem. Scr.* **1978**, *13*, 150. (f) Fraenkel, G.; Pramanik, P. *J. Chem. Soc., Chem. Commun.* **1983**, 1527.

(2) (a) Cox, R. H.; Janzen, E. G.; Harrison, W. B. *J. Magn. Reson.* **1971**, *4*, 274. (b) Hogan, R. J.; Scherr, P. A.; Weibel, A. T.; Oliver, J. P. *J. Organomet. Chem.* **1975**, *5*, 265.

(3) (a) Olah, G. A.; Hunadi, R. J. *J. Am. Chem. Soc.* **1980**, *102*, 6989. (b) Batchelor, R. J.; Birchall, T. *J. Am. Chem. Soc.* **1983**, *105*, 3848. (c) Sooriyakumaran, R.; Boudjouk, P. *J. Organomet. Chem.* **1984**, *271*, 289. (d) Lambert, J. B.; Urdameta-Perez, M. *J. Am. Chem. Soc.* **1978**, *100*, 157.

(4) (a) Buncel, E.; Venkatachalam, T. K.; Eliasson, B.; Edlund, U. *J. Am. Chem. Soc.* **1985**, *107*, 303. (b) Edlund, U.; Lejon, T.; Venkatachalam, T. K.; Buncel, E. *Ibid.* **1985**, *107*, 6408. (c) Buncel, E.; Venkatachalam, T. K.; Edlund, U.; Eliasson, B. *J. Chem. Soc., Chem. Commun.* **1984**, 1476. (d) Buncel, E.; Venkatachalam, T. K.; Edlund, U. *Can. J. Chem.* **1986**, *64*, 1674. (e) Buncel, E.; Venkatachalam, T. K.; Menon, B. C. *J. Org. Chem.* **1984**, *49*, 413. (f) Menon, B. C.; Shurvell, H. F.; Colpa, J. P.; Buncel, E. *J. Mol. Struct.* **1982**, *78*, 29. (g) Buncel, E.; Menon, B. C. *J. Am. Chem. Soc.* **1980**, *102*, 3499. (h) Buncel, E.; Menon, B. C.; Colpa, J. P. *Can. J. Chem.* **1979**, *57*, 999. (i) Edlund, U. *Org. Magn. Reson.* **1977**, *9*, 593. (j) Edlund, U. *Ibid.* **1979**, *12*, 661.

0002-7863/87/1509-5982$01.50/0